arXiv:1604.08806v2 [cs.CV] 26 May 2016

3D Interest Point Detection Based on Geometric Measures and Sparse Refinement

Xinyu Lin, Ce Zhu, Qian Zhang, Yipeng Liu

Abstract

Three dimensional (3D) interest point detection plays a fundamental role in computer vision. In this paper, we introduce a new method for detecting 3D interest points of 3D mesh models based on geometric measures and sparse refinement (GMSR). The key point of our approach is to calculate the 3D saliency measure using two novel geometric measures, which are defined in multi-scale space to effectively distinguish 3D interest points from edges and flat areas. Those points with local maxima of 3D saliency measure are selected as the candidates of 3D interest points. Finally, we utilize an l_0 norm based optimization method to refine the candidates of 3D interest points by constraining the number of 3D interest points. Numerical experiments show that the proposed GMSR based 3D interest point detector outperforms current six state-of-the-art methods for different kinds of 3D mesh models.

Keywords: 3D computer vision, 3D interest point detection, geometric properties of local surface, scale space, sparse refinement

1 Introduction

As one of the most important local features of 3D models, 3D interest points are widely used in computer vision, such as registration[1], 3D shape retrieval[2], mesh segmentation[3] and simplification[4]. Researchers have proposed various methods to extract 3D interest points from the surface of 3D mesh models over the last few decades. Most of 3D interest point detection algorithms are based on geometric methods[4, 5, 6, 7, 8, 9, 10, 11, 12, 13]. Godila and Wagan[5] converted the mesh model into a voxel grid representation and proposed a method for detecting 3D salient local features inspired by the SIFT algorithm [14]. Sipiran and Bustos[6] proposed an effective and efficient extension of the Harris operator[15] for 3D objects. Lee et al.[4] introduced mesh saliency as a measure of regional importance for 3D meshes, where they defined mesh saliency in a scale-dependent manner using a center-surround operator on Gaussian-weighted mean curvatures. Holte addressed the problem of detecting 3D interest points using a Difference-of-Normals operator [7]. Other than geometric algorithms, there are some other methods based on machine learning[16, 17, 18] and the Laplacian spectrum[19, 20, 21].

In this paper, we propose a new method for detecting 3D interest points of 3D mesh models which is represented by triangular mesh models of arbitrary topology. Two novel geometric measures are defined in multi-scale space, i.e. the distance of neighborhood rings to the tangent plane and minimal angle of normal vectors between a vertex and its first ring, which can distinguish 3D interest points from edges and flat areas effectively. Then we utilize the two geometric measures to calculate the 3D saliency measures for every evolved mesh model in multi-scale space. We utilize the product of these 3D saliency measures at different scales as the final one, which can effectively improve the 3D saliency measure of true 3D interest points and suppress the 3D saliency measure of pseudo 3D interest points. Those vertices with local maxima of 3D saliency measure are selected as the candidates of 3D interest points. Finally, we utilize an l_0 norm based optimization method to refine the 3D interest points from the candidates by constraining the number of 3D interest points.

*All the authors are with School of Electronic Engineering / Center for Robotics, University of Electronic Science and Technology of China (UESTC), Chengdu, China. (email: xinyulin@std.uestc.edu.cn; eczhu@uestc.edu.cn; zhangqian@std.uestc.edu.cn; yipengliu@uestc.edu.cn)

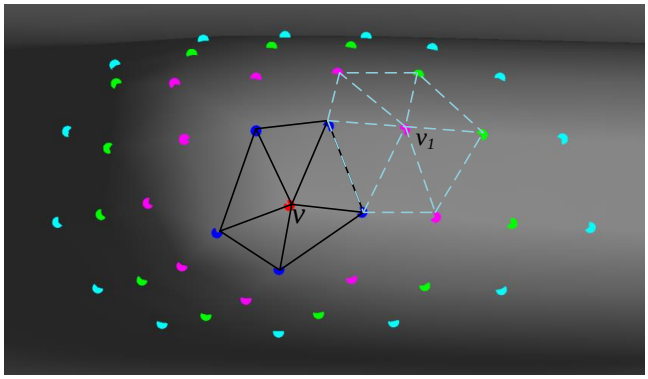

Figure 1: Vertex v and its neighborhood rings as a part of "airplane" 3D mesh model. $\boldsymbol{V}_1(v)$: blue dots; $\boldsymbol{V}_2(v)$: magenta dots; $\boldsymbol{V}_3(v)$: green dots; $\boldsymbol{V}_4(v)$: cyan dots.

In the hope of spurring further research on this significant topic, we will make our code * publicly available.

The main contributions of this paper are summarized as follows:

- Propose two novel geometric measures which can distinguish 3D interest points from edges and flat areas effectively.
- Utilize the product of 3D saliency measures as the final one to improve the 3D saliency measure of true 3D interest points and suppress 3D saliency measure of pseudo 3D interest points.
- Propose an l_0 norm based optimization method to refine the 3D interest points.

The rest of this paper is organized as follows. Section 2 introduces two novel geometric measures of local surface on a 3D mesh model. Section 3 presents our algorithm - GMSR based 3D interest point detection algorithm. Numerical experiments and results are given in Section 4. Finally, conclusions are drawn in Section 5.

2 Two Novel Geometric Measures

A 3D mesh model is represented as a set of vertices $\boldsymbol{V}$ and faces $\boldsymbol{F}$ with adjacency information between these entities. For every vertex in a triangular mesh, a list of connected vertices is able to formulate a triangle with the vertex. A vertex can have an arbitrary number of neighborhood vertices. For example, as is shown in Fig. 1, the number of the first ring around vertex v is five, but the number of the first ring around vertex v_1 is six. This topology makes the task of selecting a local neighborhood around a vertex harder.

Here, we utilize an adaptive technique in[6] to find the neighborhood of a vertex. Let v be the analyzed vertex and $\boldsymbol{V}_k(v)$ be the k-th ring around v. As is shown in Fig. 1, the first ring around vertex v, denoted as $\boldsymbol{V}_1(v)$, is made up of blue dots. Magenta dots, green dots and cyan dots form the second, third and fourth ring around vertex v respectively. For different vertices in a mesh model, they may have different number of neighborhood vertices. Based on this adaptive technique, we propose a new method using two geometric measures of the local surface to measure the regional importance for 3D mesh models: the distance of neighborhood rings to the tangent plane and the minimal angle of normal vectors between vertex v and its first ring $\boldsymbol{V}_1(v)$.

2.1 The Distance of Neighborhood Rings to the Tangent Plane

The first geometric measure used is inspired by the CPDA corner detector[22, 23], which utilized chord-to-point distance accumulation technology to replace the curvature calculation used in CSS-based corner detector[24, 25, 26]. Because an arbitrary number of neighborhood vertices can exist

*http://www.xylin.net/gmsr/

around a vertex v, we utilize the harmonic average distance of neighborhood rings to the tangent plane instead of the accumulative distance to measure the regional importance for mesh models. For every vertex v in a 3D mesh model, we utilize $\boldsymbol{n}$ to represent its normal vector. There is only one tangent plane for this vertex v. The tangent plane can be calculated by

$$\boldsymbol{n}^T[x - x_v, y - y_v, z - z_v]^T = 0 \tag{1}$$

where (x_v, y_v, z_v) is the coordinate of vertex v. Let $\overline{d_k}, k = 1, 2, 3, 4$ be the harmonic average distance of the k-th ring neighborhood vertices to the tangent plane and $\overline{d}$ be their product. We can formulate them as:

$$\overline{d} = \prod_{k=1}^{4} \overline{d_k} \tag{2}$$

$$\overline{d_k} = \frac{W_k}{\sum\limits_{j=1}^{W_k} \frac{1}{d_{kj}}} \tag{3}$$

$$d_{kj} = \frac{|\boldsymbol{n}^T[x_{kj}, y_{kj}, z_{kj}]^T - \boldsymbol{n}^T[x_v, y_v, z_v]^T|}{\|\boldsymbol{n}\|_2} \tag{4}$$

where (x_{kj}, y_{kj}, z_{kj}) is the coordinate of the j-th point in $\boldsymbol{V}_k(v), k = 1, 2, 3, 4$ and W_k is the total number of vertices in $\boldsymbol{V}_k(v)$.

According to the definitions (2)-(4) above, for any vertex v in a 3D mesh model, a small $\overline{d}$ indicates that the vertex v locates in flat areas and vice versa. Additionally, using harmonic average distance can also distinguish 3D interest points from edges to some extent. According to (3), a short d_{kj} leads to a short $\overline{d_k}$. For points on the edges, there exists one neighborhood vertex at least which has a very short distance to the tangent plane. Compared with arithmetic average and square average distance, harmonic average is more suitable to measure the regional importance for 3D mesh models.

2.2 Minimal Angle of Normal Vectors between Vertex and Its First Ring

Besides the measure mentioned above, the other one we use to further distinguish 3D interest points from edges in mesh models is the minimal angle of normal vectors between vertex v and its first ring $\boldsymbol{V}_1(v)$, which can be formulated as:

$$\theta = \min(\arccos(\frac{\boldsymbol{n}^T\boldsymbol{n}_f}{\|\boldsymbol{n}\|_2\|\boldsymbol{n}_f\|_2})) \tag{5}$$

where $\boldsymbol{n}_f$ represents the normal vector of any vertex in $\boldsymbol{V}_1(v)$. For any vertex v in edges or flat areas of a mesh model, the value of θ should be very small because there exists at least one vertex in its first ring which has the similar normal vector with the vertex v. For 3D interest points in mesh models, the value of θ should be larger relatively.

3 GMSR Based 3D Interest Point Detection Algorithm

In this section we describe the GMSR based 3D interest point detector in detail. The outline of the GMSR based detector is as follows:

- Utilize 3D Gaussian filters to construct multi-scale space for a 3D mesh model $\boldsymbol{M}(x, y, z)$ and obtain a series of evolved 3D mesh models $\boldsymbol{M}_\sigma(x, y, z)$.
- Define the 3D saliency measure based on the two geometric measures of local surface described in Section 2, and compute the 3D saliency measure for every evolved 3D mesh model $\boldsymbol{M}_\sigma(x, y, z)$ in its scale space.
- For every vertex in a 3D mesh model $\boldsymbol{M}(x, y, z)$, multiply 3D saliency measures at different scales as the final one.

- Abstract the vertices with local maxima of 3D saliency measure as candidates of 3D interest points.
- Utilize an l_0 norm based optimization method to refine the candidates of 3D interest points.

3.1 Construct Scale Space

Similar to the algorithms in[5, 8, 4], we utilize the 3D Gaussian filter to construct the multi-scale space for a mesh model. Let $\boldsymbol{M}(x, y, z)$ be a 3D mesh model and $\boldsymbol{M}_\sigma(x, y, z)$ be its corresponding 3D mesh modes in the multi-scale space. We can have the following relationships:

$$\boldsymbol{M}_\sigma(x, y, z) = \boldsymbol{M}(x, y, z) * \boldsymbol{G}(x, y, z, \sigma) \tag{6}$$

$$\boldsymbol{G}(x, y, z, \sigma) = \frac{1}{(\sqrt{2\pi}\sigma)^3} e^{-\frac{(x^2+y^2+z^2)}{2\sigma^2}} \tag{7}$$

where σ is the standard deviation of Gaussian filter. Here, we use 7 scales $\sigma \in \{0, \varepsilon, 2\varepsilon, 3\varepsilon, 4\varepsilon, 5\varepsilon, 6\varepsilon\}$, where ε amounts to 0.3% of the length of the main diagonal located in the bounding box of the model. $\sigma = 0$ indicates that it is the original mesh model.

3.2 3D Saliency Measure

Based on the two geometric measures of local surface mentioned in Section 2, we define a 3D saliency measure ρ, which enables us to extract perceptually meaningful points of interest from 3D mesh models. Different from MSCP corner detector [24], for a vertex v in a 3D mesh model, we utilize the product of 3D saliency measures at different scales as the final one, which could effectively improve the 3D saliency measure ρ of true 3D interest points and suppress the ρ of pseudo 3D interest points. For every vertex in mesh model $\boldsymbol{M}_\sigma(x, y, z)$, we use $\rho_i(j), i = 0, 1, 2, ..., 6, j = 1, 2, 3, ..., N$ to represent its 3D saliency measure in scale i. Then its final 3D saliency measure $\rho(j)$ is

$$\rho(j) = \prod_{i=0}^{6} \rho_i(j) \tag{8}$$

$$\rho_i(j) = \frac{\overline{d_i(j)}}{\|\overline{\boldsymbol{d}_i}\|_\infty} + \alpha \frac{\theta_i(j)}{\|\boldsymbol{\theta}_i\|_\infty} \tag{9}$$

where N is the total number of vertices for a 3D mesh model. $\overline{d_i(j)}$ and $\theta_i(j)$ can be obtained via (2) and (5), respectively. $\overline{\boldsymbol{d}_i}$ represents all the $\overline{d_i(j)}$ for a 3D mesh model at scale $i\varepsilon, i = 0, 1, 2, ..., 6$ and the same definition with $\boldsymbol{\theta}_i$. The first measure of (9) can distinguish non-flat areas from flat areas. Additionally, it also can distinguish 3D interest points from edges to some extent. To better suppress the edge response, the second measure is added to the 3D saliency measure. We use a linear function to represent their relationship approximately. α is a weighting factor for two kinds of measures.

3.3 Abstract Local Maxima of 3D Saliency Map

After we obtain the 3D saliency map which is made up of all the 3D saliency measures of a 3D mesh model, those vertices with local maxima of final 3D saliency measure are selected as the candidates of the 3D interest points. We compare the value of ρ for every vertex with those points in its neighborhood rings $\boldsymbol{V}_k(v), k = 1, 2, 3, 4$ and select the maximal one as the candidate of 3D interest points. Additionally, for any vertex in candidates of 3D interest points, we compare its value of $\rho_i, i = 0, 1, 2, ..., 6$ and select the i as its scale, in which ρ_i is the biggest one.

3.4 Refine the Candidates of 3D Interest Points

For candidates of 3D interest points of a 3D mesh model, there can be some vertices with small values of 3D saliency measure ρ. Similar to the hard thresholding used in [27], we utilize an l_0

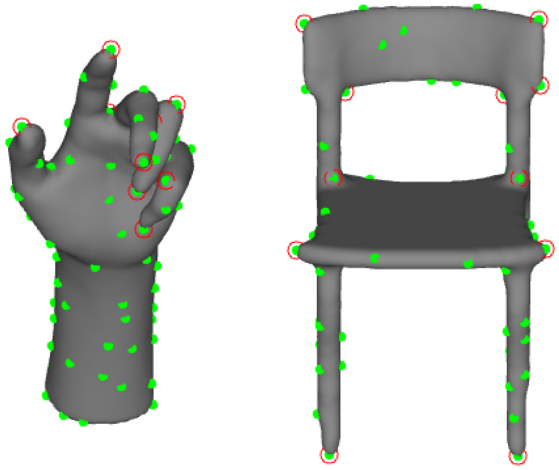

Figure 2: Green dots: the candidates of 3D interest points of two 3D mesh models. Red circles: the final 3D interest points after sparse refinement of two 3D mesh models.

norm based optimization method to refine the candidates of 3D interest points, where the vertices with low value of 3D saliency measure ρ should be eliminated. For some 3D mesh models, the 3D saliency measures $\rho(j), j = 1, 2, ..., S$ of candidates of 3D interest points are quite different. To reduce the degree of difference of $\rho(j)$ and improve the performance of the optimization model, we first perform the following mapping:

$$\rho(j) = \min(\rho(j), \frac{2}{S}\sum\nolimits_{s=1}^{S}\rho(s)) \tag{10}$$

where S represents the number of candidates of 3D interest points. Let $\boldsymbol{\rho} = [\rho(1), \rho(2), ..., \rho(S)]$ be the set of $\rho(j), j = 1, 2, ..., S$. We normalize $\boldsymbol{\rho}$, and refine it through following optimization model:

$$\begin{aligned} &\text{minimize } \beta\|\boldsymbol{x}\|_0 + \|\boldsymbol{\rho} - \boldsymbol{\rho} \odot \boldsymbol{x}\|_2^2 \\ &\text{subject to} \qquad \boldsymbol{x} = [x_1, x_2, ..., x_s] \\ &\qquad\qquad x_j \in \{0, 1\}, j = 1, 2, ..., S \end{aligned} \tag{11}$$

The first term of the target function is to constrain the number of 3D interest points. β is a penalty coefficient. The second term of the target function makes the $\boldsymbol{\rho}_{opt} = \boldsymbol{\rho} \odot \boldsymbol{x}$ close to $\boldsymbol{\rho}$ as much as possible. $\boldsymbol{\rho}_{opt}$ is the Hadamard product of $\boldsymbol{x}$ and $\boldsymbol{\rho}$. $\boldsymbol{x}$ is a vector with only two discrete elements and it has the same dimension with $\boldsymbol{\rho}$. $x_j = 0$ indicates that the j-th candidate of interest points has a low value of ρ and vice versa. We utilize a greedy algorithm to solve the optimization model according to [28]. Those points with ρ_{opt} larger than zero are selected as the final 3D interest points. As is shown in Fig. 2, green dots are the candidates of 3D interest points of two 3D mesh models and red circles are the final 3D interest points after sparse refinement of two 3D mesh models.

4 Numerical Experiments

In this section, we evaluate the performance of the GMSR based detector and compare it with six state-of-the-art 3D interest point detection algorithms - namely 3D Harris[6], HKS[9], 3D-SIFT[5], Salient Points[8], Mesh Saliency[4] and Scale Dependent Corners[10]. Our experiments are based on the publicly available benchmark [29]† where human generated ground truth data are utilized to evaluate the performance of 3D interest point detection algorithms.

†http://www.itl.nist.gov/iad/vug/sharp/benchmark/3DInterestPoint/

4.1 Datasets and Evaluation Metric

We use the same datasets as those in the benchmark [29] where a web-based application is developed and utilized to collect ground truth of interest points on 43 mesh models. These mesh models are organized in two datasets. The first one (Dataset A) is constituted by 24 triangular mesh models and annotated by 23 human subjects. The other one (Dataset B) is constituted by 43 triangular mesh models and annotated by 16 human subjects. There are two criteria while constructing the ground truth: the radius of an interest region denoted as σ and the number of human subjects n that annotated a point within that interest region. For a fixed σ, fewer ground truth points are observed as n increases since a higher consensus among human subjects is needed. For a fixed n, more ground truth points are observed as σ increases, since we accept more variation on localization of the points annotated by the human subjects.

In benchmark [29], three evaluation metrics - namely False Positive Error (FPE), False Negative Error (FNE) and Weighted Miss Error (WME) are utilized to evaluate the performance of 3D interest point detection algorithms. But FPE and FNE can be misleading in isolation as discussed in [16]. Teran [16] adopted the Intersection Over Union (IOU) [30] which combines False Positive (FP), False Negative (FN) and True Positive (TP) together as their main metric to evaluate the performance of the 3D interest point algorithms. In this paper, we also adopt the IOU metric as the evaluation metric to evaluate the performance of our proposed GMSR 3D interest point algorithm and other six state-of-the-art methods.

Let $\boldsymbol{G}_M(n,\sigma)$ be the set of ground truth points and $\boldsymbol{A}_M$ be the 3D interest points detected by an algorithm on the 3D mesh model $\boldsymbol{M}(x,y,z)$. For an interest point g in set $\boldsymbol{G}_M(n,\sigma)$, a geodesic neighbourhood of radius r is defined as $\Delta_r(g) = \{p \in \boldsymbol{M}(x,y,z) | d(g,p) \leq r\}$ where $d(g,p)$ is the geodesic distance between points g and p. The parameter r controls the localization error tolerance. A ground truth point g is correctly identified if there exists a detected point $a \in \boldsymbol{A}_M$ in $\Delta_r(g)$ and no other point in $\boldsymbol{G}_M(n,\sigma)$ closer to a. IOU at localization error tolerance r can be calculated by

$$\text{IOU}(r) = \frac{TP}{FN + FP + TP} \tag{12}$$

where $FP = N_A - N_C$ is the number of false positives and $FN = N_G - N_C$ represents the number of false negatives. $TP = N_C$ is the true positives. N_G is the number of ground truth points, N_C is the number of correctly detected points and N_A denotes the number of detected interest points by the algorithm.

4.2 Experimental Results

We display the performance results of seven algorithms on Dataset A and Dataset B in terms of IOU metric. In all experiments, parameter α in (9) is 0.5 and parameter β in (11) is 10^{-5}. The first row and the second row of Fig. 3 show the IOU curves for Dataset A and Dataset B respectively at various n/σ pairs. The first row shows the IOU curves for Dataset A with $n = 8, \sigma = 0.03$, $n = 8, \sigma = 0.05$, $n = 11, \sigma = 0.03$ and $n = 11, \sigma = 0.05$ respectively. The second row shows the IOU curves for Dataset B with $n = 2, \sigma = 0.03$, $n = 2, \sigma = 0.05$, $n = 8, \sigma = 0.03$ and $n = 8, \sigma = 0.05$ respectively. From Fig. 3, we can see that GMSR based 3D interest point detector performs best in all the situations except for one situation in Dataset B where $n = 2, \sigma = 0.05$. When localization error tolerance r is relatively large, the superiority of the GMSR based 3D interest point detection algorithm is more significant.

Fig. 4 shows some visualization results, where we display the 3D interest points of chair model in dataset A detected by the seven algorithms. Fig. 4(a) is the chair mesh model with ground truth where $n = 8, \sigma = 0.03$.

To reach an overall ranking, we calculate the average IOU score over all n/σ settings in Dataset A ($n \in \{2, 3, ..., 23\}, \sigma \in \{0.01, 0.02, ..., 0.1\}$) and Dataset B ($n \in \{2, 3, ..., 16\}, \sigma \in \{0.01, 0.02, ..., 0.1\}$). TABLE I displays the average IOU scores of Dataset A and Dataset B. We can see that GMSR based 3D interest point detector performs best in term of IOU evaluation metric.

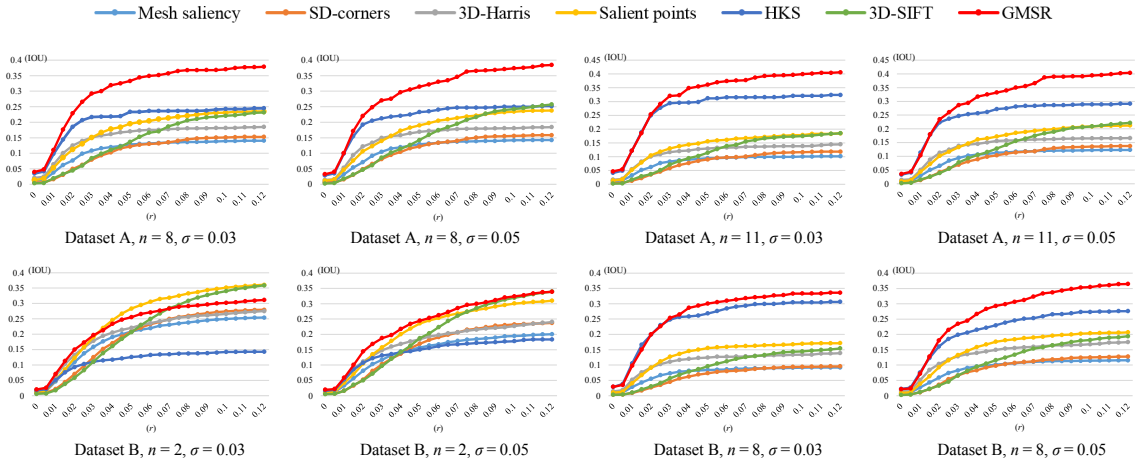
Mesh saliency
SD-corners
3D-Harris
Salient points
HKS
3D-SIFT
GMSR
(IOU)
(r)
Dataset A, $n = 8, \sigma = 0.03$
Dataset A, $n = 8, \sigma = 0.05$
Dataset A, $n = 11, \sigma = 0.03$
Dataset A, $n = 11, \sigma = 0.05$
Dataset B, $n = 2, \sigma = 0.03$
Dataset B, $n = 2, \sigma = 0.05$
Dataset B, $n = 8, \sigma = 0.03$
Dataset B, $n = 8, \sigma = 0.05$

Figure 3: Row 1 and row 2 show the IOU curves for Dataset A and Dataset B respectively at various n/σ pairs.

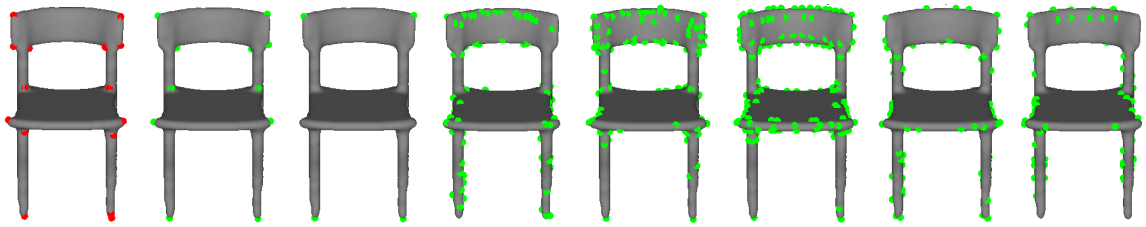

Figure 4: 3D interest points of chair model in dataset A detected by the 7 algorithms. (a) Ground truth with $n = 8, \sigma = 0.03$, (b) GMSR, (c) HKS, (d) SD-corners, (e) 3D-Harris, (e) Mesh saliency, (f) Salient points, (g) 3D-SIFT

Table 1: Average IOU on Dataset A ($n \in \{2, 3, ..., 23\}, \sigma \in \{0.01, 0.02, ..., 0.1\}$) and Dataset B ($n \in \{2, 3, ..., 16\}, \sigma \in \{0.01, 0.02, ..., 0.1\}$)

	Mesh saliency	SD-corners	3D-Harris	Salient points	HKS	3D-SIFT	GMSR
Dataset A	0.0783	0.0758	0.1044	0.1245	0.2470	0.1085	**0.2658**
Dataset B	0.0738	0.0715	0.1011	0.1244	0.2106	0.0956	**0.2224**

5 Conclusion

In this paper, we have proposed a new method for detecting 3D interest points of 3D mesh models based on geometric measures and sparse refinement. Two novel geometric measures are defined in multi-scale space to distinguish 3D interest points from edges and flat areas effectively. The first geometric measure can effectively distinguish non-flat areas from flat areas. Additionally, it can also distinguish 3D interest points from edges to some extent. To better suppress the edge response, the second geometric measure is added to the 3D saliency measure. We utilize the product of these 3D saliency measures at different scales as the final one, which can effectively improve the 3D saliency measure of true 3D interest points and suppress the 3D saliency measure of pseudo 3D interest points. Those vertices with local maxima of 3D saliency measure are selected as the candidates of 3D interest points. Finally, an l_0 norm based optimization method is used to refine 3D interest points by constraining the number of 3D interest points. Experimental results demonstrate that the GMSR based 3D interest point detector performs best in terms of IOU metric as compared to previously proposed algorithms.

References

[1] N. Gelfand, N. J. Mitra, L. J. Guibas, and H. Pottmann, "Robust global registration," in *Proceedings of the Third Eurographics Symposium on Geometry Processing*, Vienna, Austria, July 2005.

[2] T. Funkhouser and M. Kazhdan, "Shape-based retrieval and analysis of 3d models," in *ACM SIGGRAPH 2004 Course Notes*, Los Angeles, CA, USA, Aug 2004.

[3] S. Katz, G. Leifman, and A. Tal, "Mesh segmentation using feature point and core extraction," *The Visual Computer*, vol. 21, no. 8-10, pp. 649–658, 2005.

[4] C. H. Lee, A. Varshney, and D. W. Jacobs, "Mesh saliency," *ACM Transactions on Graphics*, vol. 24, no. 3, pp. 659–666, 2005.

[5] A. Godil and A. I. Wagan, "Salient local 3d features for 3d shape retrieval," *Proceedings of SPIE*, vol. 7864, pp. 78 640S–78 640S–8, 2011.

[6] I. Sipiran and B. Bustos, "Harris 3d: a robust extension of the harris operator for interest point detection on 3d meshes," *The Visual Computer*, vol. 27, no. 11, pp. 963–976, 2011.

[7] M. B. Holte, "3d interest point detection using local surface characteristics with application in action recognition," in *IEEE International Conference on Image Processing*, Paris, France, Oct 2014.

[8] U. Castellani, M. Cristani, S. Fantoni, and V. Murino, "Sparse points matching by combining 3d mesh saliency with statistical descriptors," *Computer Graphics Forum*, vol. 27, no. 2, pp. 643–652, 2008.

[9] J. Sun, M. Ovsjanikov, and L. Guibas, "A concise and provably informative multi-scale signature based on heat diffusion," *Computer Graphics Forum*, vol. 28, no. 5, pp. 1383–1392, 2009.

[10] J. Novatnack and K. Nishino, "Scale-dependent 3d geometric features," in *IEEE 11th International Conference on Computer Vision*, Rio de Janeiro, Brazil, Oct 2007.

[11] S. Wang, L. Gong, H. Zhang, Y. Zhang, H. Ren, S. M. Rhee, and H. E. Lee, "Sdtp: a robust method for interest point detection on 3d range images," *Proceedings of SPIE*, vol. 9025, pp. 90 250O–90 250O–9, 2014.

[12] E. Akagunduz and I. Ulusoy, "Scale and orientation invariant 3d interest point extraction using hk curvatures," in *IEEE 12th International Conference on Computer Vision*, Kyoto, Japan, Sept 2009.

[13] A. Mian, M. Bennamoun, and R. Owens, "On the repeatability and quality of keypoints for local feature-based 3d object retrieval from cluttered scenes," *International Journal of Computer Vision*, vol. 89, no. 2-3, pp. 348–361, 2010.

[14] D. G. Lowe, "Distinctive image features from scale-invariant keypoints," *International Journal of Computer Vision*, vol. 60, no. 2, pp. 91–110, 2004.

[15] C. Harris and M. Stephens, "A combined corner and edge detector," in *Alvey Vision Conference*, Manchester, Britain, Sept 1988.

[16] L. Teran and P. Mordohai, "3d interest point detection via discriminative learning," in *European Conference on Computer Vision*, Zurich, Switzerland, Sept 2014.

[17] C. Creusot, N. Pears, and J. Austin, "A machine-learning approach to keypoint detection and landmarking on 3d meshes," *International Journal of Computer Vision*, vol. 102, no. 1-3, pp. 146–179, 2013.

[18] S. Salti, F. Tombari, R. Spezialetti, and L. D. Stefano, "Learning a descriptor-specific 3d keypoint detector," in *IEEE International Conference on Computer Vision*, Santiago, Chile, Dec 2015.

[19] J. X. Hu and J. Hua, "Salient spectral geometric features for shape matching and retrieval," *The Visual Computer*, vol. 25, no. 5-7, pp. 667–675, 2009.

[20] R. Song, Y. H. Liu, R. R. Martin, and P. L. Rosin, "3d point of interest detection via spectral irregularity diffusion," *The Visual Computer*, vol. 29, no. 6-8, pp. 695–705, 2013.

[21] R. Song, Y. H. Liu, and Martin, "Mesh saliency via spectral processing," *ACM Transactions on Graphics*, vol. 33, no. 1, pp. 6:1–6:17, 2014.

[22] M. Awrangjeb and G. J. Lu, "Robust image corner detection based on the chord-to-point distance accumulation technique," *IEEE Transactions on Multimedia*, vol. 10, no. 6, pp. 1059–1072, 2008.

[23] M. Awrangjeb, G. Lu, C. S. Fraser, and M. Ravanbakhsh, "A fast corner detector based on the chord-to-point distance accumulation technique," in *Digital Image Computing: Techniques and Applications*, Melbourne, Australia, Dec 2009.

[24] X. H. Zhang, M. Lei, D. Yang, Y. Z. Wang, and L. T. Ma, "Multi-scale curvature product for robust image corner detection in curvature scale space," *Pattern Recognition Letters*, vol. 28, no. 5, pp. 545–554, 2007.

[25] F. Mokhtarian and R. Suomela, "Robust image corner detection through curvature scale space," *IEEE Transactions on Pattern Analysis and Machine Intelligence*, vol. 20, no. 12, pp. 1376–1381, 1998.

[26] M. Awrangjeb, G. Lu, and M. Murshed, "An affine resilient curvature scale-space corner detector," in *IEEE International Conference on Acoustics, Speech and Signal Processing*, Honolulu, Hawaii, USA, April 2007.

[27] B. Thomas and E. D. Mike, "Iterative hard thresholding for compressed sensing," *Applied and Computational Harmonic Analysis*, vol. 27, no. 3, pp. 265 – 274, 2009.

[28] J. A. Tropp, "Greed is good: algorithmic results for sparse approximation," *IEEE Transactions on Information Theory*, vol. 50, no. 10, pp. 2231–2242, 2004.

[29] H. Dutagaci, C. P. Cheung, and A. Godil, "Evaluation of 3d interest point detection techniques via human-generated ground truth," *The Visual Computer*, vol. 28, no. 9, pp. 901–917, 2012.

[30] M. Everingham, L. Van Gool, C. K. Williams, J. Winn, and A. Zisserman, "The pascal visual object classes (voc) challenge," *International Journal of Computer Vision*, vol. 88, no. 2, pp. 303–338, 2010.